ZIBELINE INTERNATIONAL PUBLISHING

ISSN: 2716-7100 (Online)
CODEN: MCEMC2

Materials & Corrosion Engineering Management (MACEM)

DOI: http://doi.org/10.26480/macem.01.2020.01.05

CrossMark

RESEARCH ARTICLE

CONSTITUTIVE MODELING OF DYNAMIC RECRYSTALLIZATION AND PRECIPITATION BEHAVIOR OF Nb AND Ti OF Q1030 HIGH STRENGTH STEEL

J.J. Wang[a], Y.L. Kang [a], Y.L. Liu[b] and H Yu[a]

[a]University of Science and Technology Beijing, China
[b]Laiwu Branch of Shandong Iron & Steel Co., Ltd., China
Corresponding Author E-mail: *bandaisuo@126.com

ARTICLE DETAILS

Article History:

Received 18 April 2020
Accepted 22 May 2020
Available online 20 June 2020

ABSTRACT

The thermal deformation and precipitation behavior at 900-1100°C and strain rate of 0.1-5s^{-1} were studied by Gleeble-3800 thermal simulator of Q1030 high strength steel. The activation energy of hot deformation in austenite region was determined by regression method, and the hot deformation equation of the Q1030 high strength steel was established. The critical strain and peak strain of dynamic recrystallization were predicted accurately by fitting the inflection point with cubic polynomial of curve of Q1030 high strength steel, and relationship between critical strain and Z parameter was established. Finally, the precipitation behavior of Nb and Ti particles during low strain rate deformation was studied, the results show that the precipitated phases in steel are rectangular TiN, quadratic (Nb, Ti) (C, N) carbonitride, elliptical (Nb, Ti) C carbide and NbC. Thermodynamic calculation shows that the order of precipitation of the second phase in steel is TiN, TiC, NbC and NbN.

KEYWORDS

thermal simulator, hot deformation, austenite region, regression method, dynamic recrystallization, cubic polynomial.

1. INTRODUCTION

Since the 1970s, the development of low-alloy high-strength steel in the world has entered a new period. Based on the control of rolling technology and microalloying metallurgy, a new concept of modern High Strenth Low Alloy Steels has been formed (Tan and Xiang, 2013; Feng et al., 2013; Liang et al., 2015; Kang et al., 2012). In recent years, a new generation of controlled rolling and controlled cooling(NG-TMCP) technology has been widely used in industrial production. In the control rolling stage, steel is used to undergo large-scale downward deformation in the austenite recrystallization area, and then tiny austenite recrystallized grains are obtained.,

The deformation is carried out in the austenite non-recrystallization area, resulting in a large number of deformation bands inside the grains. These deformation bands and austenite grain boundaries can provide nucleating points for controlling the phase transition of the cooling process. In the phase transition process, smaller ferrite or bainite tissues are produced, thereby increasing the strength and toughness of the steel (Jang et al., 2012; Li et al., 2015).

Dynamic recrystallization can change the microstructure of materials and affect their mechanical properties. It is an effective method to control the structure and performance in the process of metal thermal processing. When deformation occurs at high temperatures and high strain rates, the changes in the internal tissues of the metal are very complex, including hardening, dynamic recovery, and dynamic crystallization of austenite during deformation. These behaviors are important factors that determine the microstructure, deformation resistance, and organizational properties of the final material of the deformed austenite (Wei et al., 1997; Lan et al., 2011).

For the high-strength structural steel with low cost and high added value, the deformation behavior of austenite becomes more complicated due to the addition of Nb, V and Ti microalloy elements (Medina and Mancilia, 1993) .In this paper, the dynamic crystallization of high strength Q1030 steel is studied by means of the thermal simulation tester and the austenite crystallization thermal deformation equation is established.

The critical condition of dynamic recrystallization is studied by the cubic polynomial fitting method of the curve. The precipitation behavior of Nb and Ti nitrogen carbides at low strain rate is studied by TEM and EDX, and the theoretical basis is provided for the establishment of a reasonable hot working process.

2. EXPERIMENTAL MATERIALS AND METHODS

The test material was taken from the Q1030 high-strength steel produced by Laiwu Iron and Steel Company's wide and heavy plate production line. The chemical composition of the continuous casting slab after heating by the heating furnace is shown in Table 1. In order to preserve the state of the slabs after heating and prevent the new precipitation during the slow cooling process, the slabs are quenched into water immediately after being cut.

Quick Response Code	Access this article online	
	Website: https://macej.com.my	**DOI:** 10.26480/macem.01.2020.01.05

Cite the Article: J.J. Wang, Y.L. Kang, Y.L. Liu and H Yu (2020). Constitutive Modeling Of Dynamic Recrystallization And Precipitation Behavior Of Nb And Ti Of Q1030 High Strength Steel. *Materials & Corrosion Engineering Management, 1(1): 01-05.*

Table 1: Chemical composition of test steel (wt%).

C	Si	Mn	P	S	Al	Cr	Ti	Nb	Mo
0.055	0.18	1.18	0.016	0.003	0.042	0.51	0.120	0.042	0.21

Slab was made into many Φ 8 × 12 mm sample. They were tested on the Gleebe3800 thermal simulator and protected throughout by high purity argon. In order to make the alloy elements contained in the experimental steel as far as possible solid solution, the specimen is heated at a rate of 10°C/S to 1200°C and then keep 3 min warm to get a complete austenitic, then cooled to a different temperature at 10 °C/s. A single pass compression test of true strain 0.7 was performed, and the deformation temperature was 900°C, 950°C, 1000°C, 1050°C, 1100°C, the strain rate was 0.1 s-1, 1 s-1, 5 s-1. In order to prevent the specimen from oxidizing during the deformation process, high purity nitrogen is used as a protective gas, and graphite is coated at both ends of the specimen to reduce friction during the deformation process and prevent the occurrence of belly. The automatic sampling system records the stress and strain data of the compression deformation process. Immediately after the deformation of the sample, it is cooled with water to freeze the high-temperature austenite and precipitates. The deformed specimen was cut along the cross-sectional line to make the metallographic sample, corroded with saturated picric acid solution, and then the tissue was observed under a metallographic microscope. The samples were prepared into thin films and extracted compound specimens, and the microstructure was observed at high multiples by the H800 transmission electron microscope, and the precipitated phase components were analyzed by EDS.

3. Experimental Results and Analysis

3.1 Stress-strain curve

Figure 1 shows the true stress(σ)-strain(ε) curve of Q1030 high strength steel at different deformation temperatures and different strain rates. Fig. 1(a) is the rheological stress curve of high strength Q1030 steel at different deformation temperatures when $\bar{\varepsilon}$ =0.1s-1. It can be seen that at this strain rate, the rheological stress curve at a temperature of 950 ~ 1150°C has the characteristics of dynamic crystallized rheological stress curve. In addition, it can be seen that at the same strain rate, the peak strain and peak stress increase with the decrease of temperature.

Figure 1(b) is the rheological stress curve of high strength Q1030 steel at different strain rates at 1000°C. When the strain rate is 0.1 s-1 and 1s-1, the rheological stress curve is still of dynamic recrystallization type; When the strain rate is 5s-1, the rheological stress immediately enters a stable rheological state after reaching its peak, indicating that a dynamic recovery process occurs l at this time. It can be found that for Q1030 high strength steel, when the strain rate is small at the same deformation temperature, dynamic crystallization is easy to occur. With the increase of strain rate, peak stress and peak strain increase, the characteristics of rheological stress curve transition from dynamic recrystallization to dynamic recovery.

In the process of thermal deformation, the two mechanisms of material hardening and dynamic softening work simultaneously. At the beginning of deformation, machining hardening plays a leading role; As the deformation progresses, when the material begins to undergo dynamic crystallization, σ-ε curve is going down, and the dynamic softening mechanism plays a major role at this time; As the crystallization continues, when the hardening and dynamic softening reach equilibrium, the rheological stress σ is a certain stable value, and the material enters a complete recrystallization state.

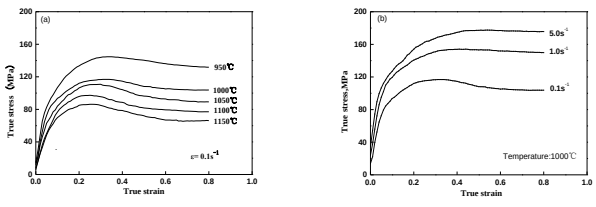

Figure 1: Rheological stress curve of Q1030 strength steel at (a) 1s-1 and at (b) 1000°C.

3.2 Thermal deformation equation

Thermal activation energy of dynamic recrystallization of metal materials is related to peak stress (σ_P), deformation temperature (T) and strain rate ($\bar{\varepsilon}$). According to the Zener-Hollomon parameter model, during the thermal deformation of nitrogen-microalloyed high-strength steel, the Z(Zener-Hollomon) parameter and the deformation activation energy Qdef, the temperature T and the strain rate $\bar{\varepsilon}$ have the following relationship (Ferdowski et al., 2014):

$$Z=\dot{\varepsilon}\exp(\frac{Q_{def}}{RT}) \quad (1)$$

In the formula, Q_{def} is the thermal deformation activation energy(kJ/mol), reflecting the ease of thermal deformation of the material; R is the gas constant with a value of 8.314J/(mol·K), $\dot{\varepsilon}$ is the strain rate(s-1), and T is the deformation temperature(K). The following relationship exists between peak stress and Z parameters (Mirzadeh et al., 2012):

$$Z=A[sinh(\alpha\sigma_p)]^n \quad (2)$$

In the formula: A is the material constant and N is the stress index; σ_P is peak stress, Single bit is MPa, α is the stress factor, and in carbon steel material, the α value is 0.012, and Combine the equations (1) and (2) to get the following equation (Fulvio and John, 2000):

$$\dot{\varepsilon}=A[\sinh(\alpha\sigma_p)]^n \exp(\frac{Q_{def}}{RT}) \quad (3)$$

Equation (3) describes the effects of deformation temperature and strain rate on the rheological stress of a metal during thermal deformation. Take the logarithm of both sides of equation (3) and take the partial derivative. The expression of heat deformation activation energy Q_{def} can be obtained:

$$Q_{def}=Rn\frac{\partial\{ln[sinh(\alpha\sigma_p)]\}}{\partial(1/T)}\Big|_{\dot{\varepsilon}}\frac{\partial ln\,\dot{\varepsilon}}{\partial ln[sinh(\alpha\sigma_p)]}\Big|_T=Rnb \quad (4)$$

When the deformation temperature(T) is certain, $\ln\dot{\varepsilon}$ and $ln[sinh(\alpha\sigma_p)]$ should satisfy the linear relationship, The relation curve between $ln\,\dot{\varepsilon}$ and $ln[sinh(\alpha\sigma_p)]$ is shown in Figure 3(a); Similarly, when the strain rate ($\bar{\varepsilon}$) is certain, 10^4T^{-1} and $ln[sinh(\alpha\sigma_p)]$ should satisfy the linear relationship, and the slope is b/10000, and the relationship curve between it is shown in Figure 3(b). Using Origin software for linear fitting, B, N and values can be obtained.

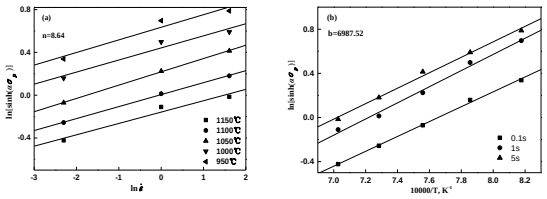

Figure 2: Relationships between strain rate (a), deformation temperature (b) and stress of Q1030 steel.

After calculation, the deformation activation energy of Q1030 high strength steel is 380.96 kJ/mol, B is 6987.52, N is 8.64. In the process of thermal deformation, by linear fitting lnZ and $\ln[\sinh(\alpha\sigma_p)]$, as shown in Fig 3, lnA = 42.678 can be obtained.

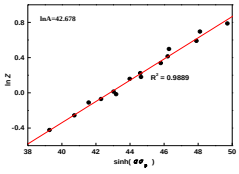

Figure 3: Relationship between Z parameter and flow stress of Q1030 high strength steel.

Then get the Z parameter:

$$Z=3.42\times10^{18}[sinh(0.012\sigma_p)]^{8.64} \quad (5)$$

The thermal deformation equation of Q1030 high-strength steel is:

$$\dot{\varepsilon}=3.42\times10^{18}[\sinh(0.012\sigma_p)]^{8.64}\exp(-\frac{380960}{8.3147}) \quad (6)$$

3.3 Critical conditions for dynamic recrystallization

The critical strain ε_c is the key to determine whether dynamic recrystallization occurs. Only when the tangible variable is greater than ε_c, the austenite will undergo dynamic crystallization. And the size of ε_c indicates the difficulty of dynamic recrystallization of austenite, so the accurate determination of ε_c is very important for the study of thermal deformation process parameters. In a general way, Usually = (0.60 ~ 0.85). In previous scientific research, researchers proposed many mathematical models to predict the critical conditions for the beginning of dynamic recrystallization, Polyak et al believed that the occurrence of dynamic recrystallization needs to satisfy two conditions: the maximum storage energy and the minimum dissipation rate, which can be expressed by the following formula (Poliak and Jonas, 2003):

$$\frac{d}{d\theta}(-\frac{d\theta}{\sigma}) \quad (7)$$

In the formula, θ is the processing hardening rate, $\theta=d\sigma/d\varepsilon$. The critical point at which dynamic recrystallization begins can be determined directly by the relationship curve with σ. And Najafizadeh-Jonas simplified the above method, A cubic polynomial is used to fit the data of work hardening, and the critical stress and critical strain are determined by curve analysis method (Najafizadeh and Jonas, 2006). In this research, a method similar to Najafizadeh-Jonas was used to determine the critical stress σ_p and critical strain ε_c of dynamic recrystallization, and the inflection point was determined by the cubic polynomial fitting of the pair and curve (Dong et al., 2000). When fitting, the strain value is limited to the peak strain, the polynomial is as follows:

$$\theta=A_1\sigma^3+A_2\sigma^2+A_3\sigma+A_4 \quad (8)$$

$$ln\,\theta=B_1\varepsilon^3+B_2\varepsilon^2+B_3\varepsilon+B_4 \quad (9)$$

In the formula, A1-A4 and B1-B4 are constants under the corresponding deformation conditions.

The second derivative of both sides of equation (8) to σ can be obtained:

$$\frac{d^2\,ln\theta}{d\sigma^2}=6A_1\sigma+2A_2 \quad (10)$$

At the critical stress at the beginning of dynamic recrystallization, the following formula holds:

$$\frac{d^2\,ln\theta}{d\sigma^2}=6A_1\sigma_c+2A_2=0 \quad (11)$$

Available:

$$\sigma_c=-A_2/(3A_1) \quad (12)$$

Similarly, it can be obtained:

$$\varepsilon_c=-B_2/(3B_1) \quad (13)$$

Take the stress-strain with a deformation temperature of 1000 °C and a strain rate of 0.1 s -1 as an example. Since the actual rheological stress curve is not a digital smooth curve, it will cause large fluctuations during analysis. Therefore, the stress-strain curve is first fitted with nine polynomial functions and then differential operations are performed. The fitting curve and its cubic polynomial fitting calculation values are shown in Figure 5. It can be seen that the calculated value and the experimental value have a high degree of quasi-coincidence, indicating that the results of the cubic polynomial fitting can be used to describe the relationship between the hardening rate and the stress and strain.

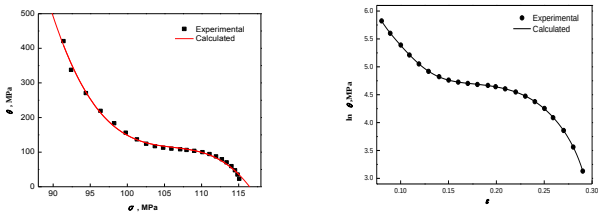

Figure 4: Curve at 1000°C and 0.1s-1 with their corresponding third order polynomial.

By fitting the cubic polynomial of the curve, we can calculate: $\varepsilon_c=0.22$; According to peak strain, it can be obtained $\frac{\varepsilon_c}{\varepsilon_p}=0.64$. With the same method, the ε_c values can be calculated at different temperatures and at different strain rates values of different temperatures and different strain rates can be calculated. According to the critical strain and peak strain data and the calculation results of Z parameters, the relationship graph of Q1030 high strength steel dynamic crystallization is drawn, as shown in Figure 5.

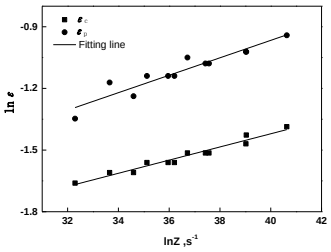

Figure 5: Dynamic recrystallization critical strain (ε_c) and its relationship with Z parameters of Q1030 steel.

It can be observed from Fig. 6 that the Z parameters can reflect the change laws of critical strain ($\ln\varepsilon_p$) and deformation conditions. The critical strain is closely related to the heat processing parameter Z value, and $\ln\varepsilon_p$ has a good linear agreement with the lnZ: The fitting function relation is obtained by linear fitting through the least square method, that is, the critical strain model:

$$\varepsilon_p=6.88\times10^{-2}Z^{0.041} \quad (14)$$

$$\varepsilon_c=6.67\times10^{-2}Z^{0.029} \quad (15)$$

3.4 Morphology and composition of Nb and Ti precipitated particles

Nb and Ti particles in Q1030 steel precipitated at the strain rate of 0.1 deformation temperature of 1000°C were studied. According to the morphology of the extracted particles, there were four main types. The first type of precipitated phase is shown in Fig. 6(a). Its shape is rectangular, about 150nm long and about 100nm wide. The composition of the precipitate is mainly TiN by EDS spectroscopy. The larger precipitated particles are observed by transmission electron microscopy. (100 nm or more), the ratio of the rectangular precipitated particles is between 20 and 30%. The second type of precipitated phase is as shown in Fig. 6(b), and the entire precipitated particle is composed of two parts: an approximately square base (A) and an attachment (B) attached to the base in an elliptical shape.

The matrix A is Ti-rich (Ti, Nb)(C, N) is analyzed by the EDS component, and the N content is slightly higher than the C content; The Elliptic attachment B is rich in Nb(Nb, Ti)(C, N), and the C content is much higher than the N content. After observation by transmission electron microscope, in larger precipitated particles (more than 100 nm), composite precipitated particles account for about 70-80%. The third precipitation phase type is shown in Figure 6(c). There is a large number of elliptical precipitated phase particles between 50nm and 80nm. After

EDS analysis, this precipitated particle is (Nb, Ti) C, but Ti content is less. The fourth type of precipitation phase type is shown in Figures 6(d) and(e). There is a kind of NbC precipitates with small size (10~20nm) and some small precipitates precipitate along dislocation.

According to the above experimental results, precipitates can be roughly divided into three categories based on the size, composition and morphology of microalloy elements: the first and second species precipitate particles are one type, most of them are over 100nm, mainly TiN, (Ti, Nb) (C, N) as shown in Fig. 6(a) and (b). The second type of precipitated particles is 50nm to 80nm in size, the oval in shape, and chemical composition is(Nb, Ti) C, but Ti content is small, as shown in Figure 6(c); The size of the third precipitates is 10nm~20nm , and the shape is also elliptical. The composition is NbC, and some particles precipitate along dislocation, as shown in Fig. 6(d) and (e).

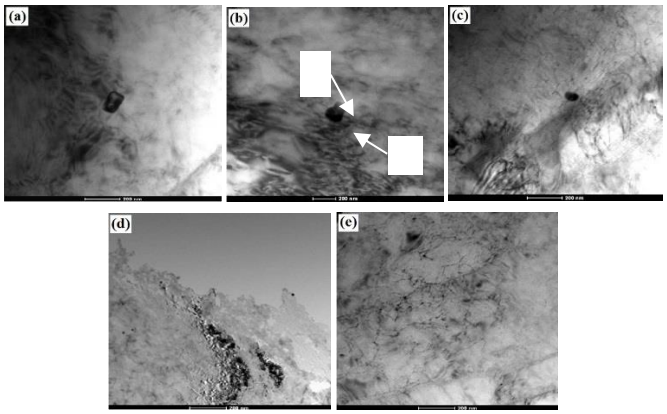

Figure 6: Morphology of precipitated particles.

3.5 Thermodynamic analysis of precipitation behavior

The precipitation of microalloy elements will lead to the decline of the free energy of the system, so the precipitation is a spontaneous process. The free energy zy of the system can be expressed as follows:

$$F = U - TS \tag{16}$$

In the formula, U is the internal energy of the system; T is the absolute temperature; S is the entropy of the system.

In the formula, since entropy S is multiplied by absolute temperature T, the contribution of entropy to free energy is relatively large at high temperature, and microalloy elements tend to dissolve. At low temperature, internal energy has a great influence on free energy while entropy is relatively small, and microalloy elements tend to precipitate to reduce internal energy (Xu et al., 2006). Therefore, with the gradual decrease of temperature, the precipitation tendency of microalloying elements gradually increases. When the temperature drops to a certain extent, microalloying elements will be precipitated in the form of carbonnitride.

Generally speaking, the precipitation of carbon nitride of microalloy elements in steel can be divided into the following three stages: the first stage is the liquid phase precipitation in the solidification process of steel billet; The second stage is the austenite precipitation after solidification and during rolling. The third stage is ferrite precipitation after γ-α phase transition after rolling (Meng et al., 2014).

Microalloy elements niobium and titanium have different affinities with carbon and nitrogen atoms, and their carbonitrides have different solubility in austenite. Their sizes can be expressed by solubility products, as shown in the following formula (Kang et al., 2006):

$$\mathrm{Lg}([Ti][N] = 0.32 - 8000/T \tag{17}$$

$$\mathrm{Lg}([Nb][N] = 3.79 - 10150/T \tag{18}$$

$$\mathrm{Lg}([Ti][C] = 2.75 - 7500/T \tag{19}$$

$$\mathrm{Lg}([Nb][C] = 2.96 - 7510/T \tag{20}$$

$$\mathrm{Lg}([Nb][C + 12/14N] = 226 - 6700/T \tag{21}$$

According to the actual composition of the steel, the equilibrium precipitation temperature of each precipitated particle was calculated as follows: TiN-1538℃, NbN -1013℃, TiC- 1164℃, NbC -1110℃, Nb(C, N) -1146℃. It can be seen that the precipitation temperature of TiN was much higher than that of other carbon nitrides, and TiN was the first precipitated in the cooling process. Due to the high precipitation temperature of TiN, TiN has enough time to grow in the subsequent cooling process, and finally forms square TiN particles with larger size (more than 100nm), as shown in Fig. 7 (a).

As the temperature continues to decrease, Nb carbonitrides gradually reach the supersaturated state and begin to precipitate. Due to the similar structure of microalloy elements Nb and Ti carbonitride, therefore, the increased strain energy and interface energy of the precipitated particles on the TiN matrix are less, the nucleation resistance is less, and the precipitation is easier to achieve (Guo, 2013). The particles of the new nucleation on the matrix grow up and have a certain diffusion miscible with the TiN Matrix, and finally form a compound precipitation particle, as shown in Fig. 7 (b). Therefore, in the controlled rolling and controlled cooling Q1030 steel, the first type of precipitated particles are composite precipitates composed of TiN which starts to nucleate in the solidification process and the particles precipitated from the upper nucleation.

In the low-temperature austenite region of steel, the content of Ti in precipitated particles is relatively low due to the large amount of Ti precipitated in the early stage. Ti is a strong solid N element, which has a strong binding force with N. Almost all the N elements are fixed by TiN formed at high temperature, and there is no N element in the particles precipitated from nucleation of austenite region at low temperature. Therefore, in the controlled rolling and controlled cooling Q1030 steel, the second type of precipitated particle is (Nb,Ti) C with separate nucleation in austenite region.

The solubility of microalloying elements in austenite is much higher than that in ferrite, therefore, after the γ-α phase transition, microalloy elements will continue to precipitate from the matrix. Due to the low temperature at this time, the resulting particles are smaller in size. as shown in Fig.7 (d) and (e). The third type of precipitates is NbC in the ferritic region.

4. Conclusions

(1) dynamic recrystallization activation energy of Q1030 high-strength steel is 380.96kJ/mol, and the thermal deformation equation can be expressed as:

$$\dot{\varepsilon} = 3.42 \times 10^{18}[\sinh(0.012\sigma_p)]^{8.64} \exp(-\frac{380960}{8.314T})$$

(2) the critical strain was obtained by using the cubic polynomial fitting of the sum curve of Q1030 high-strength steel to determine the inflection point, and the critical strain model of dynamic recrystallization was established, which can be expressed as:

$$\varepsilon_p = 6.88\times10^{-2}Z^{0.041}$$

$$\varepsilon_c = 6.67\times10^{-2}Z^{0.029}$$

(3) Tere are three types of precipitates of microalloy elements in Q1030 high-strength steel: the first type has a size of more than 100nm and a shape of regular rectangular or complex composed of rectangular matrix and elliptic attachment; The size of the second type is 50nm~80nm, the shape is oval, and the chemical composition is mainly (Nb, Ti) C. The third type is 10nm~20nm in size, oval in shape and NbC in chemical composition. Some particles precipitate along dislocation.

(4) Three types of microalloy element precipitates in Q1030 steel were formed at different stages. The first type of precipitates were TiN nucleating in the solidification process of steel, and the square TiN gradually grew to more than 100nm in the cooling process or formed composite precipitates with the particles precipitated from the upper nucleation. The second type of precipitates were (Nb, Ti) C nucleating alone in the austenite region, and the third type of precipitates were NbC nucleating in the ferritic region.

REFERENCES

Dong, J.X., J.J. Siciliano, F., Jr. 2000. Effect of Silicon on the Kinetics of Nb (C, N) Precipitation During the Hot Working of Nb- Bearing Steels ISIJ Int, 40(6), 613

Feng, R., L.L. Li, Z.S. Li. 2013. Nb-V-Ti microalloy steel complex precipitation characteristics J. Mater. Heat Treat, 2, 37-42

Ferdowsi, M.R.G., D. Nakhaie, P.H. Benhangi, G.R. Ebrahimi. 2014. Modeling the high temperature flow behavior and dynamic recrystallization kinetics of a medium carbon microalloyed steel J. Mater. Eng. Perform, 23(3), 1077-87

Fulvio, S., J.J. John. 2000. Mathematical Modeling of the Hot Strip Rolling of MicroalloyedNb Multiple-Alloyed Cr-Mo and Plain C-Mn Steels Metall. Mater. Trans, A 31A(2), 511-30

Guo, H.J. 2013. Metallurgical Physical Chemistry Course (Beijing: Metallurgical Industry Press), 171-6

Jang, J.H., C.H. Lee, Y.U. Heo, et al. 2012. Stability of (Ti, M) C (M=Nb, V, Mo and W) carbide in steels using first-principles calculations Acta Mater, 60(1), 208-17

Kang, Y.L., J. Fu, D.L. Liu, et al. 2006. Microstructure and properties control of thin slab continuous casting and rolling steel (Beijing: Metallurgical Industry Press)

Kang, Y.X., D.Y. Cai, C.H. Zhang, et al. 2012. Thermal Deformation Equation and Thermal Processing Diagram of Microcarbon Steel J. Mater. Heat Treat, 33(6), 74-9

Lan, L.Y., C.L. Qiu, D.W. Zhao, et al. 2011. Dynamic and static recrystallization behavior of low carbon high niobium microalloyed steel J. Iron Steel Res. Int, 18(1), 55-60

Li, X., L.Z.D. Wang. 2015. Interphase precipitation behavior of nanoparticles in low carbon microalloy steels containing Nb-Ti JOM-J. Met, 51(4), 417-24

Liang, H.Q., Y. Nan, Y.Q. Ning, H.Z. Guo. 2015. Correlation between strain-rate sensitivity and dynamic softening behavior during hot processing J. Alloy. Compd, 632, 478-85

Luo, Y.S., J.M. Zhang, et al. 2012. Evolution of precipitates in Nb-Ti binary low-carbon microalloyed steels J. Univ. Sci. Technol. B, 34(7), 775-82

Medina, S.F.J.E. Mancilia. 1993. Determination of static recrystallization critical temperature of austenite in microalloyed steels ISIJ Int, 33(12), 1257

Meng, Z.B., G.L. Wu, X.B. Liu, et al. 2014. Ti precipitates in Nb-Ti microalloyed high strength steel J. Mater. Heat Treat, 35(4), 106-10

Mirzadeh, H., J.M. Cabrera, A. Najafizadeh. 2012. Modeling and prediction of hot deformation flow curves Metall. Mater. Trans. A, 43(1), 108-23

Najafizadeh, A., Jonas. 2006. ISIJ Int, 46, 1679

Poliak, E.I., J.J. Jonas. 2003. Initiation of dynamic recrystallization in constant strain rate hot deformation ISIJ Int, 43(5), 684–91

Tan, Z.L., S. Xiang. 2013. Behavior of hot deformation and critical strain for dynamic recrystallization of a Q690 low carbon microalloyed steel Trans. Mater. Heat Treat, 34(5), 42-6

Wei, Y., Z.D. Wang, B. Han, et al. 1997. High-temperature deformation behavior of austenite in Nb /Ti-microalloyed steel J. North Eastern Univ.- Nat. Sci, 18(2), 165

Xu, Y.B., Y.M. Yu, D. Wu, et al. 2006. Thermodynamic Calculation of Exhalation Behavior of Nb Microalloy Steel J. Mater. Res, 20(1), 104-8.